Modeling and analysis of periodic and quasi-periodic sandwich structures with internal resonators

Marcelo A. Trindade[1], Julian J. Rimoli[2], Massimo Ruzzene[3]

[1]*Department of Mechanical Engineering, São Carlos School of Engineering, University of São Paulo, São Carlos, SP 13566-590, Brazil, trindade@sc.usp.br*
[2]*School of Aerospace Engineering, Georgia Institute of Technology, Atlanta, GA 30332, United States, julian.rimoli@aerospace.gatech.edu*
[3]*Department of Mechanical Engineering, University of Colorado Boulder, Boulder, CO 80309, United States, massimo.ruzzene@colorado.edu*

Abstract. The use of internal resonators, acting as vibration absorbers, for low-weight closed periodic structures, such as honeycomb core sandwich plates is an interesting alternative for vibration control treatments that do not rely on significant strains on the host structure. One of the main challenges for the study of such solutions is the computational cost required for their analysis, design and optimization. This work presents a modeling strategy and procedure applied for periodic and quasi-periodic sandwich structures with internal resonators aiming at reducing the required computational cost while still allowing parametric analysis, design and optimization.

Keywords: Quasi-periodic structures, Sandwich structures, Vibration control.

1 Introduction

Numerous research groups have explored the feasibility of vibration absorbers in low-weight flexible structures, including the use of distributed low-size absorbers. The use of distributed internally resonating sub-systems has expanded the applications of the original tuned mass dampers, since it allows distribution of small masses over the host structure, instead of a large concentrated mass, and may even be more effective as each absorber may be tuned to a different frequency [1]. Multiple distributed vibration absorbers also allow to explore the effect of periodicity for wave [2] and vibration [3] control. They have also been applied for vibroacoustic applications [4].

Internally resonating sub-systems may be particularly interesting for closed structures, such as sandwich, box-type and some thin-walled structures. Focused on attenuating impact loads on sandwich-type structures, the inclusion of discrete mass-spring vibration absorbers inside the core of a sandwich beam was proposed in [5]. Peng and Pai [6] discussed the design of spring-mass-damper subsystems distributed on a vibrating plate, concluding that the amount of damping in internal resonators is crucial to the vibration control performance. A latter work included dissipation in the internal vibration absorbers to reduce vibration amplitudes of a sandwich beam [7]. The same concept was considered in [8] to improve acoustic insulation properties, while maintaining the lightweight nature of sandwich plates. The use of continuous internal resonators as vibration absorbers inside a honeycomb core of sandwich plates motivated by vibration control treatments that do not rely on significant strains on the host structure, as do viscoelastic constrained layer damping treatments, was studied in [9].

Hence, there is growing interest in the use of internal resonances to improve structural vibration control, while there is still room for improvement in existing techniques and solutions, particularly due to the computational cost required for their analysis, design and optimization. Thus, a modeling strategy and procedure, based on [10, 11], is presented and applied for periodic and quasi-periodic sandwich structures with internal resonators aiming at reducing the required computational cost while still allowing parametric analysis, design and optimization. This is done using a component mode synthesis (CMS) to obtain a reduced-order model for each cell which are then assembled to build a model for the whole structure. This procedure allows to consider different properties for the resonators, leading to quasi-periodic structures that could potentially yield better vibration reduction performance.

2 Problem description

A 400x500x22 mm sandwich plate is considered (Figure 1ab). The sandwich core was considered to be made of PolyJet DM 8510 polymer with Young's modulus 2.35 GPa, Poisson's ratio 0.4, loss factor 0.01 and mass density 1160 kg m^{-3} [9]. The wall thickness of each individual core cell is 1 mm, leading to a double wall thickness of 2 mm in all but plate edges' walls (Figure 1c). The upper and lower faces are considered to be made of Aluminum with Young's modulus 70 GPa, Poisson's ratio 0.35, loss factor 0.01 and mass density 2700 kg m^{-3}.

Internal resonators, as shown in Figure 1c, for which the central mass is a cuboid with *xyz* dimensions, $5 \times 4 \times 5$ mm, the plate-like springs along the x direction are 6.5 mm long, 4 mm wide and 4 mm thick, and the plate-like springs along the y direction are 7 mm long, 5 mm wide and 4 mm thick, are inserted in the sandwich core cells. Other geometries for the internal resonators, respecting the constraints posed by the sandwich core voids, can be considered. They are supposed to be 3D-printed together with the square core walls in a 3D printer capable of printing two different materials simultaneously as in [9]. The resonators (both mass and plate-like springs) are to be made of PolyJet DM 9860, which is a much softer digital polymer compared to DM 8510 and with a reasonably high loss factor. Its properties are: mass density 1130 kg m^{-3}, Young's modulus 3.605 MPa, Poisson's ratio 0.4 and loss factor ranging between 0.05 and 0.30 (here, a loss factor of 0.10 will be considered) [9].

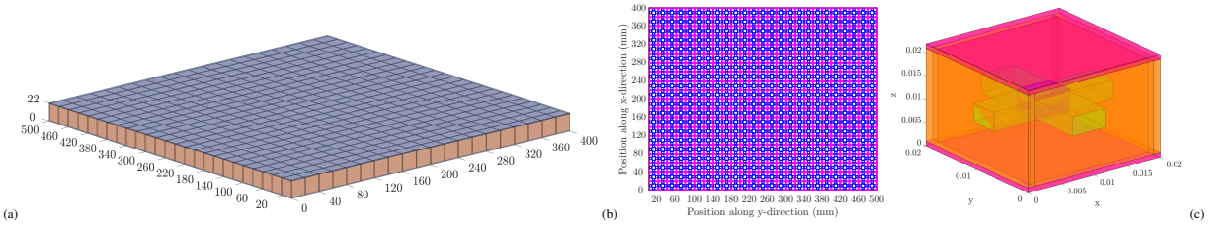

Figure 1. Schematic representation of the sandwich plate with square core and internal resonators.

3 Finite element modeling of a single cell

The sandwich individual cell has dimensions 20x20x22 mm and was modeled using a finite element (FE) model, with 20-node isoparametric solid elements for all volumes (faces, core walls and resonator's mass and plate-like springs). A total of 3180 elements, 21149 nodes and 63447 degrees-of-freedom (dofs) was obtained for the case depicted in Figure 1c. To account for the loss factor in the resonator, a viscoelastic complex modulus approach was considered, such that the Young's and shear moduli for the DM 9860 material are written, respectively, as $Y^* = Y^R(1+\mathrm{i}\eta_Y)$ and $G^* = G^R(1+\mathrm{i}\eta_G)$. For simplicity, an isotropic material with constant properties is considered, such that $G^R = Y^R/[2(1+\nu)]$ and $\eta_Y = \eta_G = \eta$. This leads to the following equations of motion for the cell

$$\left(-\omega^2\mathbf{M}_c + \mathbf{K}_c^*\right)\mathbf{u} = \mathbf{F}, \text{ with } \mathbf{K}_c^* = \mathbf{K}_c^R + \mathrm{i}\mathbf{K}_c^I, \tag{1}$$

in which $\mathbf{u}$ are the nodal displacements amplitudes in the three Cartesian directions.

This model is saved for each resonator design and later used for assembling the full sandwich plate. Here, a CMS will be considered in order to obtain a reduced-order model for each cell and, thus, a less computationally expensive model for the full plate. For that, constraint and flexible normal modes are computed for the cell. Also, to guarantee full displacement continuity between adjacent cells, the interface (or surface) nodes not retained in the global scale model, sometimes called hanging nodes, are interpolated based on the retained ones.

First, boundary, surface and interior dofs, $\mathbf{u}_b$, $\mathbf{u}_s$ and $\mathbf{u}_i$, are defined. Different boundary meshing refinement may be considered. Here, the nodal displacements at the 20 nodes usually considered in a solid quadratic isoparametric FE, as shown in Figure 2, are considered in $\mathbf{u}_b$, leading to 60 boundary dofs. The other nodal displacements on the X^-, X^+, Y^- and Y^+ surfaces, which will be connected to adjacent cells, will be named $\mathbf{u}_s$. The remaining nodal displacements will be considered as interior/internal dofs $\mathbf{u}_i$. Then, (1) is rewritten as

$$\left\{-\omega^2\begin{bmatrix}\mathbf{M}_{bb} & \mathbf{M}_{bs} & \mathbf{M}_{bi}\\ \mathbf{M}_{sb} & \mathbf{M}_{ss} & \mathbf{M}_{si}\\ \mathbf{M}_{ib} & \mathbf{M}_{is} & \mathbf{M}_{ii}\end{bmatrix} + \begin{bmatrix}\mathbf{K}^*_{bb} & \mathbf{K}^*_{bs} & \mathbf{K}^*_{bi}\\ \mathbf{K}^*_{sb} & \mathbf{K}^*_{ss} & \mathbf{K}^*_{si}\\ \mathbf{K}^*_{ib} & \mathbf{K}^*_{is} & \mathbf{K}^*_{ii}\end{bmatrix}\right\}\begin{bmatrix}\mathbf{u}_b\\ \mathbf{u}_s\\ \mathbf{u}_i\end{bmatrix} = \begin{bmatrix}\mathbf{F}_b\\ \mathbf{0}\\ \mathbf{0}\end{bmatrix}. \tag{2}$$

The non-retained surface dofs are interpolated from the boundary dofs using quadratic shape functions and considering the entire cell as the domain, such that $\mathbf{u}_s = \mathbf{N}_{sb}\mathbf{u}_b$. Each line of $\mathbf{N}_{sb}$ is evaluated for each surface node in terms of its cartesian coordinates. Then, constraint modes are obtained assuming imposed unitary boundary

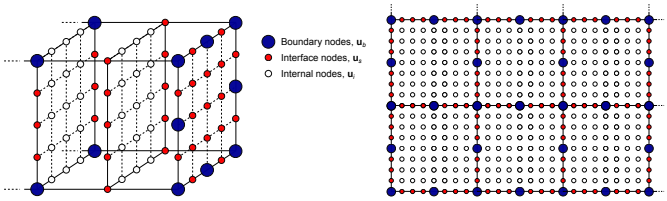

Figure 2. Schematic representation of boundary, surface/interface and interior/internal nodes considered in the component mode synthesis procedure: partial 3D view of a cell (left) and top view of connected cells (right).

displacements and neglecting the effect of damping and inertia in (2). Notice that imposed boundary displacements also lead to corresponding surface displacements according to the predefined interpolation. Thus, the internal displacements are given as $\mathbf{u}_i = -[\mathbf{K}_{ii}^R]^{-1}(\mathbf{K}_{ib}^R + \mathbf{K}_{is}^R\mathbf{N}_{sb})\mathbf{u}_b$. A matrix of constraint modes is then defined as

$$\mathbf{T}_C = \begin{bmatrix} \mathbf{I} \\ \mathbf{N}_{sb} \\ -[\mathbf{K}_{ii}^R]^{-1}(\mathbf{K}_{ib}^R + \mathbf{K}_{is}^R\mathbf{N}_{sb}) \end{bmatrix}. \tag{3}$$

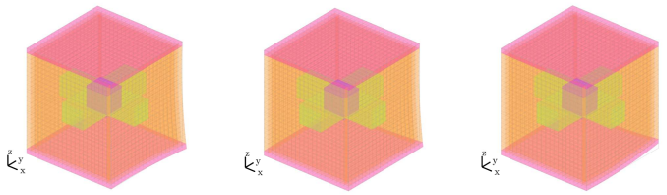

Figure 3. Three constraint modes for the cell structure.

Figure 3 shows three of the constraint modes, in which unitary displacements in the three directions are imposed in the FE node at (20,0,0) mm. Moreover, for dynamic problems and in particular for cases with internal resonances, one must account also for the cells' dynamic responses. One possible strategy could be to replace the 'static' constraint modes by 'dynamic' ones, by using the dynamic stiffness instead of the elastic one, leading to frequency dependent constraint modes which are computationally expensive to obtain. A less expensive alternative is obtained by enriching the projection basis with flexible normal modes of the cell. These are obtained by locking boundary displacements and solving the remaining eigenproblem for a given N_f flexible modes and frequencies,

$$\left(-\omega_j^2\mathbf{M}_{ii} + \mathbf{K}_{ii}^R\right)\boldsymbol{\phi}_{fj} = \mathbf{0};\ \text{with}\ \boldsymbol{\phi}_{fj}^{\mathrm{t}}\mathbf{M}_{ii}\boldsymbol{\phi}_{fj} = 1\ \text{and}\ \Omega = \mathrm{diag}(\omega_1,\ldots,\omega_{N_f}). \tag{4}$$

These flexible normal modes are such that the boundary displacements vanish and, thus, the following set can be used to enrich the projection basis by keeping some (N_f) 'internal' dofs in the reduced-order model,

$$\mathbf{T}_N = \begin{bmatrix} \mathbf{0} \\ \mathbf{0} \\ \boldsymbol{\phi}_f \end{bmatrix};\ \boldsymbol{\phi}_f = \begin{bmatrix} \boldsymbol{\phi}_{f1} & \cdots & \boldsymbol{\phi}_{fN_f} \end{bmatrix}. \tag{5}$$

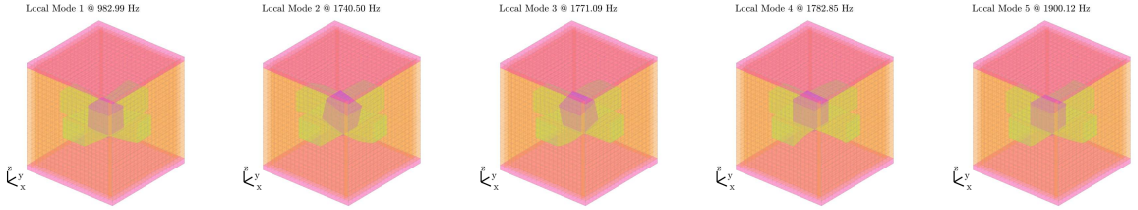

Figure 4. First five flexible normal modes for the cell structure.

The number N_f of internal dofs kept in the model depends on the frequency band of interest. Standard practice is to keep a number of flexible modes such that the maximum local natural frequency is within the frequency band of interest. Figure 4 shows the first five flexible normal modes of the cell. However, other criteria based on the

contribution of the internal dofs to the observed dynamics, as measured for example by the coupling between these dofs and boundary dofs in the assemble model, can be used. Thus, the enriched projection basis may be defined as

$$\mathbf{T} = \begin{bmatrix} \mathbf{T}_C & \mathbf{T}_N \end{bmatrix}. \tag{6}$$

Here, the first five flexible modes were kept, leading to a local model with 65 dofs (60 boundary dofs plus 5 internal dofs), which is a substantial reduction if compared to the cell's original FE model with more than 60,000 dofs. Other reduced-order models may have a larger number of dofs depending on the number of boundary dofs and kept flexible modes. But, it is clear that the reduction may easily be substantial while allowing modeling the cell in fine detail. One should note however that the number of internal dofs is multiplied by the number of cells in the full structure later on, which is why a relatively small number of internal dofs should be kept.

Then, reduced-order mass and stiffness matrices are evaluated by projecting onto the enriched basis $\mathbf{T}$,

$$\mathbf{M}_r = \mathbf{T}^{\mathrm{t}}\mathbf{M}\mathbf{T}\ ,\ \mathbf{K}_r^* = \mathbf{T}^{\mathrm{t}}\mathbf{K}^*\mathbf{T}. \tag{7}$$

Notice that the complex stiffness matrix is used, leading to a complex reduced-order matrix. Thus, although it is assumed here that the damping, represented by the imaginary part of the original stiffness matrix, $\mathbf{K}_c^I$, is small enough to allow projection onto an undamped projection basis, its contribution is kept in the reduced-order model.

4 Assembling and modal analysis of the global structure

The reduced-order model for each designed cell may then be assembled to obtain a model for the entire structure. This may be done by considering continuity in displacements for the common boundaries of adjacent cells. Here, the standard procedure used in FE to assemble the cells is considered. Notice that, since the 'hanging' interface dofs are interpolated from the kept boundary dofs, the displacement continuity between the interfaces of adjacent cells is guaranteed over the entire interface. The cells' complex stiffness matrices will lead to a complex global stiffness matrices, for which the real and imaginary parts are identified, such that

$$\mathbf{M}_g = \sum_e \mathbf{M}_r,\ \mathbf{K}_g^* = \sum_e \mathbf{K}_r^* = \mathbf{K}_g^R + \mathrm{i}\mathbf{K}_g^I. \tag{8}$$

The results presented here consider a plate structure with dimensions 400x500x22 and, thus, composed of 500 cells (20x25). This leads to a global model with 12334 dofs (9834 boundary dofs and 2500 internal dofs).

Boundary conditions may be applied to the boundary dofs of the global structure. Here, the plate is clamped in all edges (CCCC) and, thus, all 1150 boundary dofs at the edges of the sandwich plate, $x = \{0, L_x\}$, $y = \{0, L_y\}$, are locked. The number of boundary dofs is reduced to 11184. The number of internal dofs does not change.

The assembled model is then used to evaluate the natural modes and frequencies and the frequency response of the global structure. Again, to reduce the computational cost, an undamped eigenproblem is solved by considering only the real part of the global stiffness matrix $\mathbf{K}_g^R$. The effective damping due to the imaginary part $\mathbf{K}_g^I$ will be estimated in the suite. Thus,

$$\left(-\omega_j^2\mathbf{M}_g + \mathbf{K}_g^R\right)\boldsymbol{\phi}_j = 0. \tag{9}$$

Both mass and stiffness matrices are symmetric with good sparsity properties and, thus, computationally efficient methods may be used to solve for the first M natural frequencies. However, since the cells' resonators are designed to have their N_f natural frequencies within the frequency band of interest, one should expect an increase of N_f times the number of cells in the natural frequencies to be evaluated ($M > 2500$ in the present case). Therefore, this is potentially the major lever for the computational cost of the analysis. The first seven natural frequencies of the global structure without resonators are $\{797, 1231, 1455, 1788, 1805, 2243, 2261\}$ Hz.

Despite having considered only the real part of the global stiffness matrix for the evaluation of the natural modes and frequencies of the global structure, it is important to estimate the potential amount of damping added to the global structure by the internal resonators. As a first attempt, the Modal Strain Energy method is considered, in which the damping factors of the global structure are approximated by the ratio between the projection of the imaginary part of the global stiffness matrix on the global modes and that of the real part, such that

$$\zeta_j \approx \frac{\boldsymbol{\phi}_j^{\mathrm{t}}\mathbf{K}_g^I\boldsymbol{\phi}_j}{2\omega_j^2}. \tag{10}$$

This approximation could potentially be improved by enriching the global projection basis with a first-order correction based on the displacements caused by the forces generated by the imaginary part of the stiffness matrix when the structure vibrates in each undamped normal mode [12, 13]. This will be accounted for in the future.

5 Analysis of the frequency responses for periodic and quasi-periodic structures

The frequency response function (FRF) is evaluated neglecting coupling between modes due to internal damping, such that modal superposition can be used. Then, the mobility FRF can be written as

$$H(\omega) = \sum_j \frac{\mathrm{i}\omega \mathbf{c}\boldsymbol{\phi}_j \boldsymbol{\phi}_j^{\mathrm{t}} \mathbf{b}}{-\omega^2 + \mathrm{i}2\zeta_j\omega_j\omega + \omega_j^2}. \tag{11}$$

The mobility FRF shown in Figure 5 considered a point transversal force applied near the lower-left corner of the sandwich plate and an average of absolute transversal displacements at cell corners. It shows a significant effect of internal resonators on the structure's response, especially near the cells' natural frequencies (vertical dashed lines). The maximum response amplitude is reduced by 10 dB within a frequency range from 0 to 2000 Hz, which encompasses the first five natural frequencies of the host structure. The amplitude around these frequencies are respectively reduced by 9, 11, 7, 10 and 10 dB. The resonators do not affect much the response in the higher frequencies range. It is clear that the resonators' design and distribution greatly affect the vibration reduction, mainly due to the resonators' natural frequencies leading to potential band-gaps, the resonators' damping leading to an effective added modal damping, and the coupling between resonators and structure's vibration modes.

An analysis of the natural frequencies shows that the internal resonators lead to band gaps that are relatively narrow, which is expected since the mass added by the internal resonators is small. The total added mass m_R is 332.2 g, compared to a 2.0498 kg mass m_H of the host sandwich structure. This leads to a relative mass increase $\mu = m_R/m_H$ of 16.2%. Three band gaps are obtained near the resonators' natural frequencies, at $\omega_c = \{983,\ 1783,\ 1900\}$Hz, with widths $\Delta\omega/\omega_c = \{11.5,\ 1.5,\ 17.3\}$%. But, only the first one is observed in the FRF.

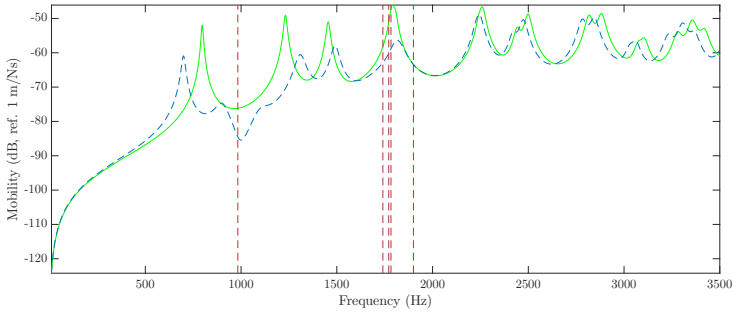

Figure 5. Mobility FRF of CCCC sandwich plate considering input at (80,80) mm and an averaged output.

The distributions of displacement amplitudes on the sandwich plate at particular excitation frequencies are shown in Figure 6. A uniform scale is used to provide a relative comparison between amplitudes. In addition, a color scale is used to represent how the individual resonators work at each frequency. For that, one color is used for each local flexible mode (modal displacement amplitude) of the resonators. Since all modal displacement amplitudes may be non null, whenever this is the case, their respective colors are combined leading to a continuous color grading. For instance, if the cell color is closer to red, the resonator inside this cell oscillates mostly in its first local flexible mode. In Figure 6, it is possible to observe that near the first resonators' natural frequency, at 983 Hz, the amplitudes are much smaller all over the plate and are concentrated around the excitation position. The resonators oscillate mostly in their first local resonance. In the frequency range defined by the other four local resonances, between 1740 Hz and 1900 Hz, the second and third local resonances importances are increased. In particular, in cells that present larger rotations around y, the second local resonance amplitude (in green) is greater, where in cell that present larger rotation around x, the third local resonance amplitude (in blue) is greater.

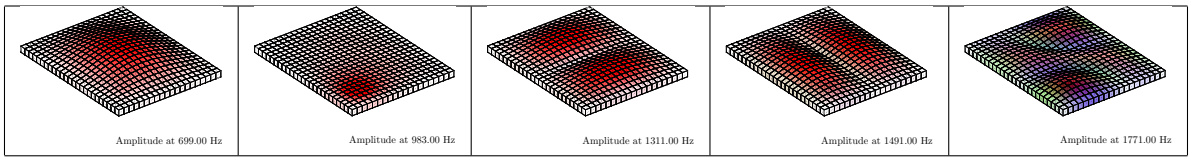

Figure 6. Displacement amplitudes on the plate and relative magnitude of resonators modal displacements.

A second analysis was performed to evaluate the potential benefits of inserting properly distributed resonators with different modal properties motivated by the ability to tune the resonators to a selection of vibration modes to be controlled. As a first distribution strategy, an additional resonator type tuned at a lower frequency was included to help reducing the vibration amplitude around the first vibration mode. This leads to a quasi-periodic structure

due to the small variations on the internal resonators. To determine the distribution of the two resonator types, the modal displacements of the first three vibration modes were evaluated for the host structure (without resonators). For the locations (cells) with greater contribution of the first mode, in the central part of the plate, the resonator type tuned to the first natural frequency was considered. A schematic representation of resonators' distribution is shown in Figure 7. To decrease the resonance frequencies of the additional resonator type tuned to the first vibration mode, it was chosen to increase its central mass height from 5 mm to 6 mm and decrease its plates thicknesses from 4 mm to 3 mm. The geometry of the two resonators is shown in Figure 8.

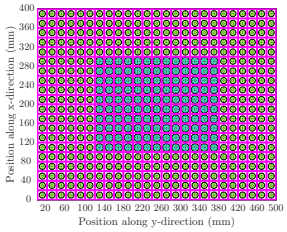

Figure 7. Resonators' distribution based on modal contributions (larger circles correspond to resonator type with smaller resonance frequencies).

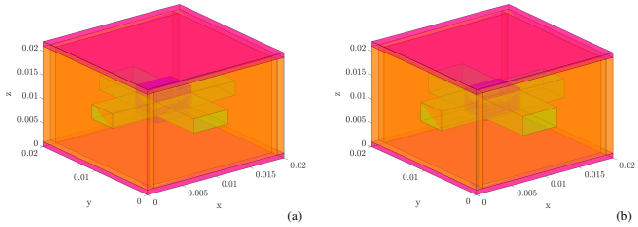

Figure 8. Representative cell of the sandwich plate with the two internal resonators types designed for smaller (a) and larger (b) natural frequencies.

The mobility FRF for the quasi-periodic case is presented in Figure 9 and shows that it was possible to improve substantially the vibration amplitude reduction around the first mode without worsening much that reduction around the remaining modes. Besides, the relative mass increase is reduced to 15.5% (total added mass of 317.2 g) since the lower frequency resonator is lighter due to thinner resonator plate-like springs. The amplitude reduction obtained around the first five original natural frequencies is respectively: 17, 10, 6, 10 and 10 dB. The reduction in the maximum amplitude within the frequency range from 0 to 2000 Hz is kept at around 10 dB.

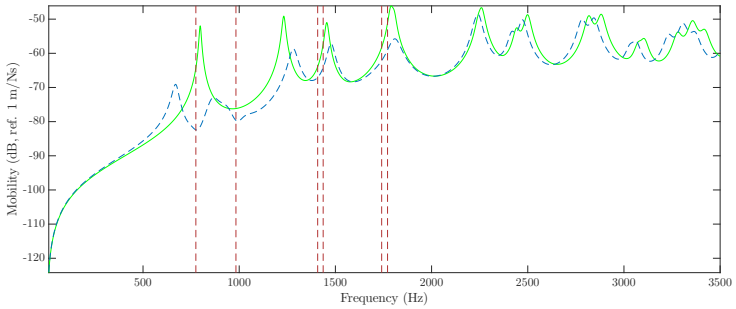

Figure 9. Mobility FRF of CCCC sandwich plate considering input at (80,80) mm and an averaged output for the quasi-periodic case with two resonator types.

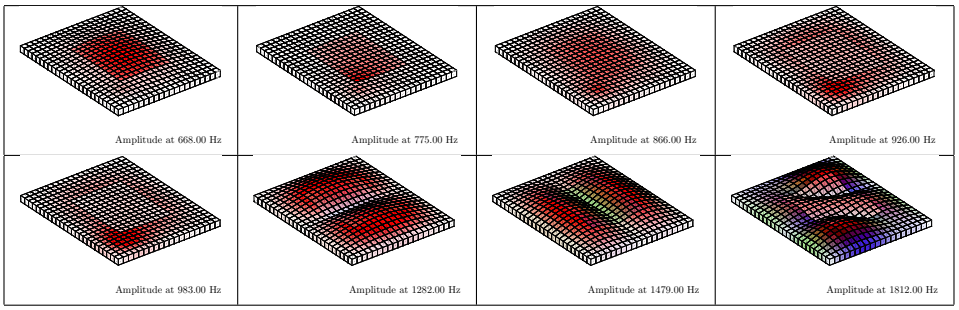

Figure 10. Distribution of displacement amplitudes on the sandwich plate and relative magnitude of resonators modal displacement for the quasi-periodic case with two resonator types.

The distributions of displacement amplitudes at particular excitation frequencies for the quasi-periodic case are shown in Figure 10. A color scale is still used to represent the response of the individual resonators. Now, they correspond to similar mode shapes but with different natural frequencies depending on the resonator properties. Hence, the three local resonances of the resonators occur at six different frequencies, 775, 1408 and 1436 Hz for the resonators with larger mass and smaller stiffness, and 983, 1740 and 1771 Hz for the resonators with smaller

mass and larger stiffness. Since now there are two resonator types distributed along the plate, with resonators with larger mass concentrated in the central portion of the plate, at any given excitation frequency, one might see each resonator type responding differently. Thus, in Figure 10, the displacement amplitude distributions are shown for excitation frequencies near the peak frequencies, but also near the first local resonances of the each resonator type (775 Hz and 983 Hz). The first five distributions in Figure 10 correspond to an excitation frequency that is near to the host structure first natural frequency. Those at 668, 866 and 926 Hz correspond to peak frequencies for the structure with resonators. In the first one (at 668 Hz), the response is concentrated at the larger mass resonators. In the second one (at 866 Hz), both resonator types are working, and in the third one (at 926 Hz), the response is mainly concentrated at the resonators with smaller mass. For other frequencies, corresponding to the second, third and coupled fourth/fifth modes, all resonators respond but in different mode shapes.

6 Conclusions

The analyses performed have shown that CMS is an interesting alternative to allow fine modeling of the individual cells with internal resonators while keeping a reasonable computational cost for the analyses of the global (assembled) structure. It was also observed that the presence of more than one resonators' resonance frequencies within the frequency range of interest may be interesting to provide a larger bandwidth vibration reduction performance and/or to allow damping of relatively distant resonance peaks simultaneously. For that, the resonators should be properly designed based on available information on the host structure resonance peaks of interest. The analyses also suggest that it is harder to make good use of individual band gaps in the host structure's low frequency range since the modal density is already low. The effective frequency range and/or width of the band gaps can also be improved by increasing the mass added by the resonators. However, in the present case, the added mass was limited to low values since the sandwich structures considered are supposed to be lightweight.

Acknowledgements. Financial support of The São Paulo Research Foundation (FAPESP), grants 2018/25989-9 and 2018/15894-0, and the National Council for Scientific and Technological Development (CNPq), grants 309193/2014-1 and 309001/2018-8, is gratefully acknowledged.

Authorship statement. The authors hereby confirm that they are the sole liable persons responsible for the authorship of this work, and that all material that has been herein included as part of the present paper is either the property (and authorship) of the authors, or has the permission of the owners to be included here.

References

[1] T. Igusa and K. Xu. Vibration control using multiple tuned mass dampers. *Journal of Sound and Vibration*, vol. 175, n. 4, pp. 491–503, 1994.
[2] P. Frank Pai. Metamaterial-based broadband elastic wave absorber. *Journal of Intelligent Material Systems and Structures*, vol. 21, n. 5, pp. 517–528, 2010.
[3] K. K. Reichl and D. J. Inman. Lumped mass model of a 1D metastructure for vibration suppression with no additional mass. *Journal of Sound and Vibration*, vol. 403, pp. 75–89, 2017.
[4] C. Claeys, E. Deckers, B. Pluymers, and W. Desmet. A lightweight vibro-acoustic metamaterial demonstrator: Numerical and experimental investigation. *Mechanical Systems and Signal Processing*, vol. 70-71, pp. 853–880, 2016.
[5] B. Sharma and C. T. Sun. Impact load mitigation in sandwich beams using local resonators. *Journal of Sandwich Structures and Materials*, vol. 18, n. 1, pp. 50–64, 2016.
[6] H. Peng and P. Frank Pai. Acoustic metamaterial plates for elastic wave absorption and structural vibration suppression. *International Journal of Mechanical Sciences*, vol. 89, pp. 350–361, 2014.
[7] H. Chen, X. P. Li, Y. Y. Chen, and G. L. Huang. Wave propagation and absorption of sandwich beams containing interior dissipative multi-resonators. *Ultrasonics*, vol. 76, pp. 99–108, 2017.
[8] Z. Liu, R. Rumpler, and L. Feng. Broadband locally resonant metamaterial sandwich plate for improved noise insulation in the coincidence region. *Composite Structures*, vol. 200, n. April, pp. 165–172, 2018.
[9] T. Yu and G. A. Lesieutre. Damping of sandwich panels via three-dimensional manufactured multimode metamaterial core. *AIAA Journal*, vol. 55, n. 4, pp. 1440–1449, 2017.
[10] F. Casadei, J. Rimoli, and M. Ruzzene. Multiscale finite element analysis of wave propagation in periodic solids. *Finite Elements in Analysis and Design*, vol. 108, pp. 81–95, 2016.
[11] G. Capuano, M. Ruzzene, and J. Rimoli. Modal-based finite elements for efficient wave propagation analysis. *Finite Elements in Analysis and Design*, vol. 145, pp. 10–19, 2018.
[12] H. Pinault, E. Arlaud, and E. Balmès. A general superelement generation strategy for piecewise periodic media. *Journal of Sound and Vibration*, vol. 469, pp. 115133, 2020.
[13] L. Rouleau. *Modélisation vibro-acoustique de structures sandwich munies de matériaux visco-élastiques*. Doctoral thesis, Conservatoire National des Arts et Métiers, Paris, France, 2013.